Dissolution of rare-earth clusters in SiO2 by Al codoping: A microscopic model

Lægsgaard, Jesper

Published in:
Physical Review B (Condensed Matter and Materials Physics)

Link to article, DOI:
10.1103/PhysRevB.65.174114

Publication date:
2002

Document Version
Publisher's PDF, also known as Version of record

Dissolution of rare-earth clusters in SiO_2 by Al codoping: A microscopic model

J. Lægsgaard
Research Center COM, Technical University of Denmark, Building 345v, DK-2800 Kongens Lyngby, Denmark
(Received 14 June 2001; published 29 April 2002)

A microscopic model for the incorporation of Er_2O_3 units in silica codoped with Al_2O_3 is presented. The model assumes that Er clustering is counteracted by the formation of Er-Al complexes in which each Er ion provides valence compensation for three substitutional Al ions. These complexes are investigated by theoretical calculations within the framework of density functional theory. Bond lengths and coordination numbers for Er and Al are in good agreement with results from extended x-ray absorption fine structure spectroscopy. The total energy of the Er-Al complexes is slightly higher than that of the phase-separated state, but thermodynamic arguments show that they are favored by entropy considerations and will prevail for sufficiently high values of the Al/Er ratio and a fictitious temperature parameter controlling the entropy contribution to the free energy of the glass. An analysis of the Kohn-Sham eigenvalue spectrum and the electrostatic potential around the dissolved Er ion provides only limited support for the approximations commonly made in the discussion of ligand-field effects.

DOI: 10.1103/PhysRevB.65.174114 PACS number(s): 61.72.Ji, 61.72.Ww, 64.75.+g

I. INTRODUCTION

The incorporation of rare-earth (RE) elements in silica glass, especially Er and Nd, has become a technologically important process over the last decade, due to the possibility of creating silica-based optical amplifiers. It is usually of high importance for the fabrication of such devices to avoid the RE cluster formation caused by the low solubility of rare earths in silica. For glass which is purely RE-doped this sets an unacceptably low concentration limit of around 10^{18} cm^{-3}.[1,2] However, it has been found that the Er solubility is greatly enhanced if the glass is simultaneously codoped with Al and/or P ions. Especially Al codoping has proven very effective, ensuring essentially complete cluster dissolution at Er concentrations above 10^{19} cm^{-3} when the Al/Er ratio is around 10 or higher.[1,3] No clear microscopic explanation for this effect exists at the moment. Arai and co-workers introduced the ''solvation-shell'' model based on the observation that rare earths are soluble in alumina but not in silica.[4] It would then seem reasonable to assume that the Al codopant atoms form some kind of solvation shell around the RE atoms. Using the electron-spin-echo envelope-modulation method of pulsed electron paramagnetic resonance (ESEEM-EPR) to detect the interaction between the magnetic moments of the Al nuclei and the $4f$ shell of Nd impurities in Nd/Al-doped silica glass, these authors demonstrated that Al codopant ions were in fact correlated to Nd, at a distance of about 3 Å.[5] On the other hand, in purely Al-doped silica Al is usually not found to form clusters, and a recent study of Nd/Al-doped glass using the technique of extended x-ray absorption fine structure (EXAFS) found no discernible change of the local Al environment between Nd/Al and pure Al doping.[6] This suggests that the local environment of the Al impurities does not change significantly when forming complexes with RE ions, and also (since no Nd coordination shell could be resolved in the Al EXAFS spectra) that only a fraction of the Al impurities are close to the rare earths. It thus seems unlikely that the solvation shells of Arai *et al.* are simply alumina nanoclusters. In fact it was speculated by Sen[6] that each RE ion is correlated to only three substitutional Al ions, as required for charge balancing. This, however, raises an additional puzzle: Experience has shown that an atomic Al/RE ratio of about 10 is usually necessary to ensure good dissolution of RE clusters in silica. If only a fraction of these Al ions form complexes with rare earths, one is led to speculate why no way of reducing the required Al/RE ratio has been found.

The low solubility of rare earths in silica is due to the mismatch in size and valence between the RE ions and the constituents of the silica network. Er may be taken as a typical example: In compounds such as Er_2O_3 and $Er_2Si_2O_7$, the Er^{3+} ions are bonded to six O atoms, with bond lengths around 2.2–2.3 Å. Thus, assuming purely ionic bonding for a moment, an Er ion would donate half an electron to each of its O neighbors. However, since a tetrahedrally coordinated Si^{4+} ion (which is known to be the common Si state in amorphous silica at ordinary pressure conditions) would donate one electron to each O neighbor, the ErO_6 unit fits poorly into a pure silica network, even when allowing for local reconstructions, and energy is therefore gained by forming clusters in which several Er ions can share nearest neighbors. On the other hand, if Al_2O_3 impurity units are also present in the glass, a new possibility arises: It is well known that the Al^{3+} ion substitutes readily for Si provided that the difference in valence electron number is compensated in some way. If three substitutional Al ions are situated close to each other, the compensating charge may be provided by an Er ion, which can easily be accomodated in the interstitial regions of the silica network.

The purpose of the present paper is to study a particular realization of this structural concept by means of density functional theory (DFT). Geometric and energetic results will be compared with available experimental information in order to clarify whether this model constitutes a plausible mechanism for RE cluster dissolution in Al-doped silica. Furthermore, electronic structures and electrostatic potentials around the rare earth ion (here taken to be Er) will be analyzed in order to shed light on various assumptions com-

monly made when discussing optical spectra of rare earths in solid materials.

The rest of the paper is organized as follows: Sec. II introduces the structural models and numerical methods used, while in Sec. III the results are presented and discussed. Conclusions are summarized in Sec. IV.

II. THEORETICAL APPROACH

In order to investigate the influence of Er-Al complexes on cluster formation three kinds of structural models are needed: One for the state of clustered Er ions in the absence of Al, one for the Er-Al complex, and finally one for the state of Al impurities in the absence of Er. Throughout this paper it will be assumed that the stoichiometry of the combined system is $x\mathrm{SiO_2}:y\mathrm{Al_2O_3}:z\mathrm{Er_2O_3}$. With the presence of sufficient O to oxidize all cation species, formation of pure-Er clusters in the solid appears unlikely. Rather, one must assume the clusters to consist of Er, or Er-Si, oxides. As models for such clusters I will use crystalline $\mathrm{Er_2O_3}$ and $\mathrm{Er_2Si_2O_7}$, respectively. This approach neglects the complicated problem of cluster surface effects in an amorphous silica network, meaning that the kinetics of cluster growth cannot be modeled. Only the thermodynamical balance between large Er clusters and dispersed Er-Al complexes can be studied.

Concerning the structure of Er-Al complexes, it is clear that the structural concept outlined in the introduction has a multitude of possible realizations. However, one can arrive at a fairly generic model geometry by considering the six-membered ring structure, which is not only common to most crystalline $\mathrm{SiO_2}$ allotropes but is also thought to be one of the dominant structural objects in amorphous silica. If every second Si atom in such a ring is substituted with Al ions, and the missing valence electrons are supplied by an Er ion in the center of the ring, the local geometry around the Er ion can be made to resemble that in the Er oxides with only minor relaxations of the $\mathrm{SiO_2}$ matrix. The geometry, which will hereafter be denoted $[\mathrm{ErAl_3O_6}]$, is schematically shown in Fig. 1(a).

Since both Al and Er are trivalent ions in silica, one can set up a structural model for the incorporation of Al in the absence of Er simply by replacing the interstitial Er ion in Fig. 1(a) by a fourth Al ion. I shall denote this structure $[\mathrm{Al_4O_6}]$. In calculations which will be detailed in a separate paper[7] I have found that this is indeed a likely geometry for Al ions in silica at concentrations above 0.1%. However, in the case of interstitial Al, the structures schematically depicted in Figs. 1(b) and 1(c) were both found to have similar total energies. In the case of interstitial Er, on the other hand, the geometry in Fig. 1(a) was clearly favored compared with other distributions of the substitutional Al ions in the ring. This can be ascribed to the larger size of the Er ion, which means that it needs more space and more neighbors than Al. The local structure of the Er and Al interstitials will be discussed further in the next section.

The electronic structure of the various impurity states in $\mathrm{SiO_2}$ considered here is described by means of the Perdew-Wang 1991 approximation[8] to DFT.[9,10] The impurities are incorporated in a 72-atom α-quartz supercell, and the Kohn-Sham wave functions are expanded in a plane-wave basis using Vanderbilt's ultrasoft pseudopotential (US-PP) approach.[11,12] The Er pseudopotential is constructed treating the $4f$ manifold as a core shell with an occupation number of 11.[13] Most calculations are performed with a plane-wave ex-

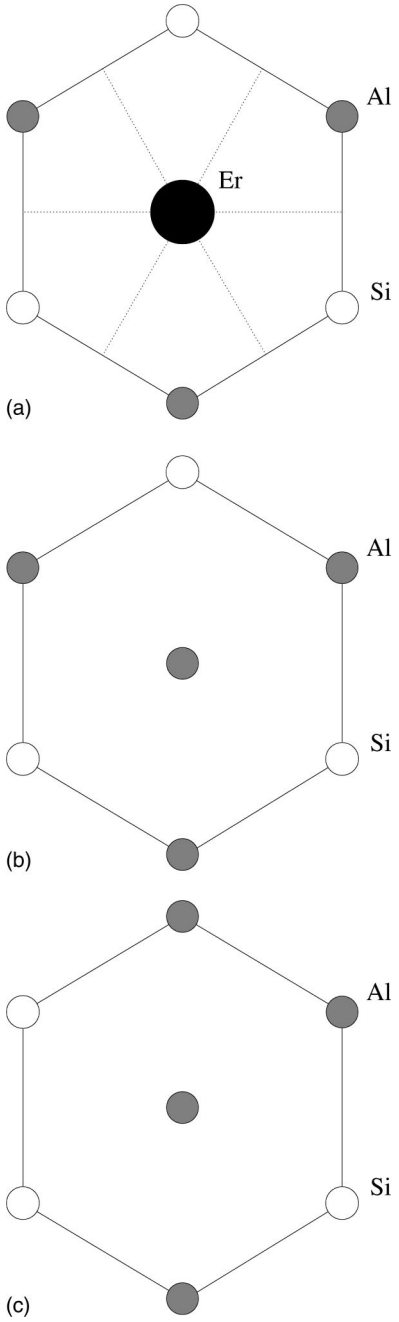

FIG. 1. Schematic representations of various $\mathrm{Er_2O_3}$ and $\mathrm{Al_2O_3}$ states in a silica network. The O atoms interconnecting the cations have been suppressed. In (a) the bonds between the rare-earth and the O atoms in the ring have been indicated by dashed lines, but it should be noted that the Er atom in the DFT calculations also bonds to O atoms outside the ring. This is also the case for the ''interstitial'' Al atom in (b) and (c) which is found to be fivefold coordinated in the (b) geometry and fourfold coordinated in the (c) geometry.

pansion cutoff at 340 eV (25 Ry), and Brillouin zone sampling is done using the Γ point only. However, since the evaluation of formation energy differences described below requires comparison of energies in different unit cells, care must be taken to avoid errors from basis set truncation. Therefore, the total energies of the relaxed structures were recalculated at cutoffs of 500 and 600 eV, at which the formation energy differences appeared to be well converged. The atomic coordinates were relaxed by means of a conjugate-gradient algorithm, which searches for the nearest local energy minimum in configuration space. A truly global optimization (through, e.g., simulated annealing) at the moment appears computationally prohibitive.

From the total energy results of the supercell calculations formation energies may be calculated for the different impurity species:

$$E_0[\mathrm{Er_2O_3}] = E^{\mathrm{sol}}[\mathrm{Er_2O_3}] - 2E^{\mathrm{at}}[\mathrm{Er}] - 3E^{\mathrm{at}}[\mathrm{O}], \quad (1)$$

$$E_0[\mathrm{Er_2Si_2O_7}] = E^{\mathrm{sol}}[\mathrm{Er_2Si_2O_7}] - 2E^{\mathrm{sol}}[\mathrm{SiO_2}] - 2E^{\mathrm{at}}[\mathrm{Er}] - 3E^{\mathrm{at}}[\mathrm{O}], \quad (2)$$

$$E_0[\mathrm{ErAl_3O_6}] = E^{\mathrm{sol}}[\mathrm{ErAl_3O_6}] - E^{\mathrm{at}}[\mathrm{Er}] - 3E^{\mathrm{at}}[\mathrm{Al}] - 6E^{\mathrm{at}}[\mathrm{O}] - 21E^{\mathrm{sol}}[\mathrm{SiO_2}], \quad (3)$$

$$E_0[\mathrm{Al_4O_6}] = E^{\mathrm{sol}}[\mathrm{Al_4O_6}] - 4E^{\mathrm{at}}[\mathrm{Al}] - 6E^{\mathrm{at}}[\mathrm{O}] - 21E^{\mathrm{sol}}[\mathrm{SiO_2}]. \quad (4)$$

Here E^{sol} are DFT energies calculated in the solid state, while the E^{at} are energies of free (pseudo) atoms. For the impurity complexes E^{sol} is the energy of the α-quartz supercell, whereas for the crystalline phases E^{sol} is taken as the energy per formula unit at the theoretical equilibrium volume with all internal parameters relaxed. In the supercell with 24 SiO_2 units substitution of three Si ions leaves 21 SiO_2 units in addition to the $[\mathrm{ErAl_3O_6}]$ or $[\mathrm{Al_4O_6}]$ unit. $E^{\mathrm{sol}}[\mathrm{SiO_2}]$ is the energy per SiO_2 unit of pure silica calculated using the same supercell and calculational parameters as for the impurity calculations in order to eliminate systematic errors. The choice of atomic reference energies is not of significance in the present work since only differences of formation energies between various states in the condensed phase will be needed. I will consider the energy difference between two limiting cases: In the ''clustered'' phase, all Er ions are present in large Er_2O_3 or $Er_2Si_2O_7$ clusters and all Al impurities are in $[\mathrm{Al_4O_6}]$ states. In the ''dissolved'' phase, all Er ions are in $[\mathrm{ErAl_3O_6}]$ states and only the remaining Al impurities form $[\mathrm{Al_4O_6}]$ complexes (it is assumed that the ratio, r, between the Al_2O_3 and Er_2O_3 concentrations is always greater than 3). In the limit of low impurity concentration the energy difference per Er_2O_3 unit between the two phases is given by

$$\begin{aligned}\Delta E &= E_0[\mathrm{Er_2O_3}] + \tfrac{3}{2}E_0[\mathrm{Al_4O_6}] - 2E_0[\mathrm{ErAl_3O_6}] \\ &= E^{\mathrm{sol}}[\mathrm{Er_2O_3}] + \tfrac{3}{2}(E^{\mathrm{sol}}[\mathrm{Al_4O_6}] - 21E^{\mathrm{sol}}[\mathrm{SiO_2}]) \\ &\quad - 2(E^{\mathrm{sol}}[\mathrm{ErAl_3O_6}] - 21E^{\mathrm{sol}}[\mathrm{SiO_2}]) \end{aligned} \quad (5)$$

if the clusters are assumed to consist of Er_2O_3 crystallites. In the case of $Er_2Si_2O_7$ clusters one finds

$$\begin{aligned}\Delta E &= E_0[\mathrm{Er_2Si_2O_7}] + \tfrac{3}{2}E_0[\mathrm{Al_4O_6}] - 2E_0[\mathrm{ErAl_3O_6}] \\ &= E^{\mathrm{sol}}[\mathrm{Er_2Si_2O_7}] + \tfrac{3}{2}(E^{\mathrm{sol}}[\mathrm{Al_4O_6}] - 21E^{\mathrm{sol}}[\mathrm{SiO_2}]) \\ &\quad - 2(E^{\mathrm{sol}}[\mathrm{ErAl_3O_6}] - 20E^{\mathrm{sol}}[\mathrm{SiO_2}]). \end{aligned} \quad (6)$$

It will also be of interest to evaluate the energy required for changing the occupation of the Er $4f$ multiplet in the $[\mathrm{ErAl_3O_6}]$ structure. To this end, I construct new pseudopotentials with an f occupancy of 10 or 12 and a corresponding change in the number of valence electrons. I hereafter calculate the total energy of the $[\mathrm{ErAl_3O_6}]$ geometry, relaxed in the f^{11} configuration, with these new pseudopotentials. Of course, the pseudopotentials do not properly describe the ''internal'' energy of the $4f$ multiplet at different occupation numbers in a reliable way: They are only intended to give a good description of core-valence interactions. However, an estimate of the true energy difference can be obtained by the expression

$$E_{f^{12}} - E_{f^{11}} = (E^{\mathrm{at}}_{f^{12}} - E^{\mathrm{at}}_{f^{11}}) + (\tilde{E}^{\mathrm{sol}}_{f^{12}} - \tilde{E}^{\mathrm{sol}}_{f^{11}}) - (\tilde{E}^{\mathrm{at}}_{f^{12}} - \tilde{E}^{\mathrm{at}}_{f^{11}}) \quad (7)$$

and similarly for the f^{11}-f^{10} excitations. Here $E, \tilde{E}$ denote all-electron and pseudo-total-energies, respectively. The first term in parentheses gives an estimate of the energy required to take a free Er atom from the f^{11} to the f^{12} configuration, while the remaining terms gives the difference in the energy required to place the free Er atom in the $[\mathrm{ErAl_3O_6}]$ structure between f^{11} and f^{12} configurations. The all-electron free-atom calculations in the different configurations are performed within the generalized gradient approximation (GGA) without spin polarization. Thus, the present approach neglects the multiplet structure of the $4f$ manifold, and should be considered as an average estimate of the energy difference between the various J states possible for each value of the f occupation number.

The US-PP approach can be regarded as an approximation to the projector augmented wave function (PAW) method developed by Blöchl,[14,15] in which the Kohn-Sham wave functions of the solid are expanded in augmented plane waves according to

$$\Psi_{n\mathbf{k}\sigma} = \tilde{\Psi}_{n\mathbf{k}\sigma} + \sum_i \langle \tilde{\Psi}_{n\mathbf{k}\sigma} | \beta_i \rangle (\phi_i - \tilde{\phi}_i). \quad (8)$$

Here $\Psi_{n\mathbf{k}\sigma}$ is a smooth pseudo-wave-function that can be expanded in plane waves, and β_i is a set of projector functions that are duals to the soft atomic pseudo-wave-functions $\tilde{\phi}_i$ which match the true atomic orbitals ϕ_i outside a chosen pseudization radius around each atom. The idea behind the method is that the $\langle \tilde{\Psi}_{n\mathbf{k}\sigma} | \beta_i \rangle \tilde{\phi}_i$ terms cancel the pseudo-wave-function inside the pseudization spheres leaving only the expansion of the ''hard'' atomic orbitals ϕ_i. n,

and σ are band and spin indices, respectively, while i is a combined spin, angular momentum, and main quantum number index. All of these functions are present in both the PAW and US-PP schemes. Therefore, from the results of a US-PP calculation a hard wave function can be reconstructed using Eq. (8). In this work I shall use this reconstructed wave function to obtain projected state densities according to

$$\rho_l^i(\omega)=\sum_{n\mathbf{k}}\sum_{pqm}\langle\phi_{plm}^i|\phi_{qlm}^i\rangle \times\langle\beta_{qlm}^i|\tilde{\Psi}_{n\mathbf{k}\sigma}\rangle\langle\tilde{\Psi}_{n\mathbf{k}\sigma}|\beta_{plm}^i\rangle\delta(\omega-\varepsilon_{n\mathbf{k}}). \quad (9)$$

In this formula i is an atom index, while pq and lm are main and angular momentum quantum numbers, respectively. Spin indices have been suppressed. This wave function will also be used to analyze the electrostatic (Hartree) potential around the Er ion. When calculating this potential I represent the bare ions as point charges balancing the valence electron charge of the atom in question, that is, the variation of the potential due to the finite extent of the core orbitals is not taken into account.

III. NUMERICAL RESULTS AND DISCUSSION

A. Equilibrium structures

The relaxed structure of the $[ErAl_3O_6]$ complex is shown in Fig. 2(a). Apart from Er, only the ions of the surrounding six-member ring and the additional O atoms bonded to Er have been included. The local correlation function around the Er ion is shown in Fig. 2(b), where each neighbor site has been broadened by a Gaussian with a dispersion of 0.01 Å^2 to smoothen the curves. There are seven O atoms in the nearest neighbor shell at distances of 2.23–2.55 Å and one extra O atom at a distance of 2.79 Å. The average and dispersion of the bond lengths (without the Gaussian broadening) are given in Table I, and compared to experimental results from an EXAFS study of SiO_2-TiO_2 glass codoped with 9% $AlO_{1.5}$ and 0.5% $ErO_{1.5}$.[16] The agreement with the theoretical results is quite good, but it should be noted that the present theory does not account for the effect of TiO_2 codoping. Only the seven nearest O neighbors have been included in the theoretical average, since they appear to form a reasonably well separated shell in Fig. 2(b). In his study of Al/Nd-doped silica Sen found a Nd coordination of 8 and an average bond length of 2.62 Å.[6] The Er and Nd bond lengths are not comparable due to the effect of the lanthanide contraction. However, it appears to be a general trend in both theory and experiments that the RE-O bond lengths in the SiO_2 matrix are larger than in the rare earth oxide materials [the average bond length in Nd_2O_3 is 2.47 Å (Ref. 6)]. Concerning the more distant neighbors the appearance of a Si-Al-O shell around 2.8 Å in the present calculation seems problematic, since such a shell to my knowledge has not been identified in EXAFS experiments. However, the difference in intermediate-range environment between α quartz and amorphous silica may influence the results, so further studies based on other silica allotropes or models of the amorphous environment will be needed here. In addition, it might be interesting to analyze existing EXAFS data again based on the bond length distributions found in the present work.

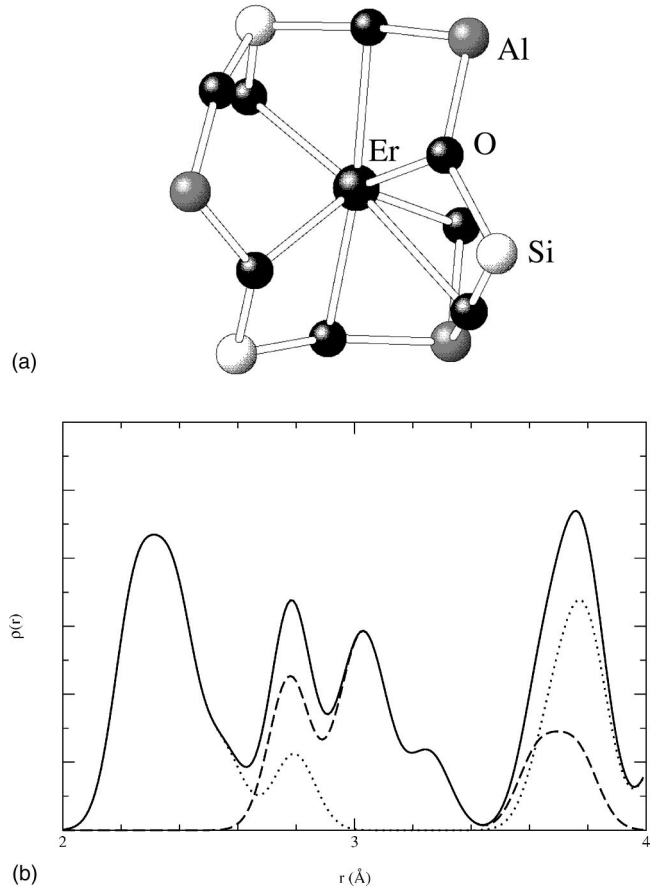

FIG. 2. Local environment around the Er ion in the relaxed $[ErAl_3O_6]$ geometry. In (a), the atomic geometry is shown. White spheres represent Si, gray Al, small black O and large black Er. In (b) an Er-centered correlation function obtained by Gaussian broadening of the near-neighbor distances is plotted. The full line gives the total correlation function, and the dotted and dashed lines are Er-O and Er-(Si,Al) projections, respectively.

The Al ions in the $[ErAl_3O_6]$ state have four O neighbors at an average distance of 1.75 Å, and a second coordination shell of four Si atoms at an average distance of 3.2 Å, in addition to the Er atom, which is 2.78–3.26 Å away from the Al ions. These values are in good agreement with the EXAFS data of Sen,[6] who obtained first- and second-shell radii of 1.77 and 3.12 Å, respectively. As discussed above, the absence of a distinguishable RE peak in the Al EXAFS signal may be ascribed to the fact that the number of Si and O neighbors is much higher and that only a fraction of the Al ions form complexes with the rare earths. In the $[Al_4O_6]$ structures the mean Al bond length is 1.77 Å for the structure in Fig. 1(b) and 1.80 Å for that in Fig. 1(c). The slight increase in the bond lengths can be explained by the fact that the interstitial Al ion has longer bonds than the substitutional ones. This is especially the case for the structure in Fig. 1(c) where the interstitial Al turns out to be fivefold coordinated, whereas in the structure shown in Fig. 1(b) the interstitial Al is fourfold coordinated. From these results one would not

TABLE I. Total energies, coordination numbers (Z), bond length average, and bond length dispersion of the Er states considered. The total energies of the clustered phases relative to a phase with dissolved Er in $[ErAl_3O_6]$ complexes are given for Er_2O_3 and $Er_2Si_2O_7$ clusters as calculated from Eqs. (5) and (6), respectively, with a plane-wave cutoff of 600 eV.

Er state	$\Delta E/Er_2O_3$ (eV)	Z	d_{av} (Å)	$\langle d^2\rangle - d_{av}^2$ (Å^2)
$[ErAl_3O_6]$	—	7	2.35	0.011
Expt. (Ref. 16)	—	7.4 ± 0.8	2.31 ± 0.04	0.013 ± 0.003
Er_2O_3	0.50	6	2.28	0.0008
$Er_2Si_2O_7$	−0.36	6	2.28	0.0006

expect an observable change in the Al EXAFS spectra upon rare-earth doping, in accordance with the results of Sen.

B. Total energy results and thermodynamic models

The total energy differences between the Er-Al complex and the Er cluster models considered are summarized in Table I. The phase separated limit represented by the $Er_2Si_2O_7$ system is seen to constitute the energy minimum. However, the difference between this state and $[ErAl_3O_6]$ is quite small, and the latter is favored by entropy considerations, since the Er atoms are dissolved. Whether, and how, thermodynamic arguments can be applied to glassy systems is a delicate question, which depends on the fabrication process of the glass. It is commonly believed that melt-quenched glass can be considered a frozen-in state corresponding to a fictitious temperature somewhat below the melting point ($\sim$2000 K for silica), but other fabrication methods, such as plasma-enhanced chemical vapor deposition (PECVD) or the sol-gel technique, do not involve such high temperatures. With these methods, the Er clustering is usually only observed during subsequent annealing steps (necessary to produce glass of high transparency), at lower temperatures (for PECVD, anneals at $\sim$1200 K are typical). Assuming that the anneal time is sufficiently long to allow for local redistributions, through diffusion processes, over scales larger than the average distance between impurities, it would seem reasonable to assume that the impurity state distribution over lattice sites corresponds to a thermodynamical equilibrium at the anneal temperature, but this may not always be fulfilled in practice. Nevertheless, I shall describe the entropy effects by using standard thermodynamic considerations since this is the only way to obtain simple analytical estimates of the impurity behavior as a function of concentration and temperature. At ambient conditions, where pressure effects are unimportant in the condensed phase, it is sufficient to consider the Helmholz free energy of the system in the clustered and dissolved phases. In the limit of low impurity concentration the total free energy of the system can be written as a sum of free energies for the individual species (in this case $[ErAl_3O_6]$, $[Al_4O_6]$, and $Er_2Si_2O_7$ cluster complexes), which under the above assumptions is given by the formula

$$F[i]=N_i\left\{E_0[i]+kT\left[\ln\left(\frac{c_i}{x_i}\right)-1\right]\right\}. \tag{10}$$

Here $F[i]$ is the total free energy for species i, c_i is the concentration measured in number of i complexes per cation site (at low impurity concentrations the number of cation sites, $N_{cat}\sim N_{Si}$), and x_i specifies the number of available states per cation site for complexes of type i. N_i is the total number of complexes of type i (that is, $N_i=c_iN_{cat}$), and $E_0[i]$ is the formation energy per formula unit of complex i. Experiments monitoring Er clustering at temperatures around 1400 K found mean cluster radii of 10–20 nm without indications of a saturating growth process.[2] At such radii, each cluster will contain thousands of Er_2O_3 units, and the entropy per Er_2O_3 unit will be negligible. Thus, it seems reasonable to assume $F=E_0[Er_2Si_2O_7]$ (as for complete phase separation) in the clustered phase. The free energy of the $[ErAl_3O_6]$ complexes in the dissolved state is

$$F[ErAl_3O_6]=N_{Er}\left\{E_0[ErAl_3O_6]+kT\left[\ln\left(\frac{c_{Er}}{x_{Er}}\right)-1\right]\right\}, \tag{11}$$

where N_{Er} is the total number of Er ions in the system, c_{Er} the corresponding concentration, and x_{Er} the $[ErAl_3O_6]$ degeneracy parameter (number of available states per cation site). Finally, the free energies associated with the $[Al_4O_6]$ complexes in the clustered and dissolved phases are

$$F^{cl}[Al_4O_6]=\frac{N_{Al}}{4}\left\{E_0[Al_4O_6]+kT\left[\ln\left(\frac{c_{Al}}{4x_{Al}}\right)-1\right]\right\}, \tag{12}$$

$$F^{diss}[Al_4O_6]=\frac{N_{Al}-3N_{Er}}{4}\left\{E_0[Al_4O_6]+kT\left[\ln\left(\frac{c_{Al}-3c_{Er}}{4x_{Al}}\right)-1\right]\right\}, \tag{13}$$

where the parameters N_{Al}, c_{Al}, etc., are defined in a similar manner as for Er. The formulas reflect the fact that the number of Al ions available for $[Al_4O_6]$ formation is reduced by a factor of $3N_{Er}$ when the Er ions are dissolved in $[ErAl_3O_6]$ states. Now the total free energy per Er_2O_3 unit of the two phases can be expressed as

$$F^{cl}=E_0[Er_2Si_2O_7]+\frac{2}{N_{Er}}F^{cl}[Al_4O_6], \tag{14}$$

$$F^{diss}=\frac{2}{N_{Er}}F[ErAl_3O_6]+\frac{2}{N_{Er}}F^{diss}[Al_4O_6]. \tag{15}$$

Recalling that r is the ratio between the Al and Er impurity concentrations, the free energy difference becomes

$$\Delta F=\Delta E+\frac{3kT}{2}\left[\ln\left(\frac{r-3}{2}\right)+\ln\left(\frac{x_{Er}}{2x_{Al}}\right)\right]-\frac{kT}{2}\left[\ln\left(\frac{2c_{Er_2O_3}}{x_{Er}}\right)+r\ln\left(1-\frac{3}{r}\right)-1\right]. \tag{16}$$

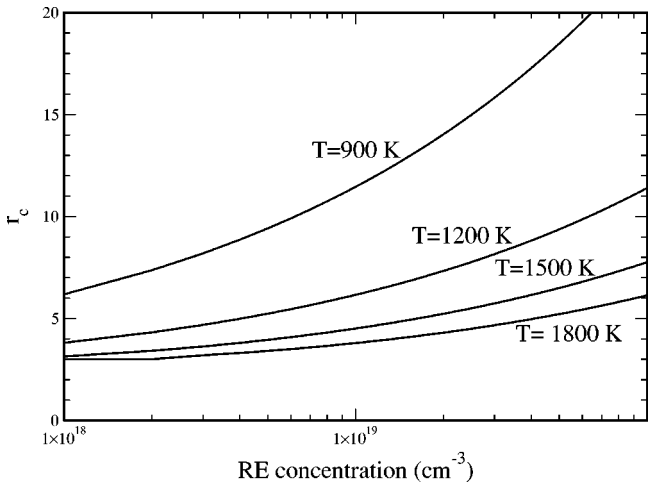

FIG. 3. Critical values of the Al/RE ratio obtained by requiring the free energy difference in Eq. (16) to be zero for different values of the temperature parameter. The Er concentrations are converted to cm^{-3} assuming a density of 2.21 gm/cm^3 for pure silica glass.

Here ΔE and ΔF are, respectively, the total and free energy difference per Er_2O_3 unit between the two phases. The ΔE parameter for $Er_2Si_2O_7$ clusters can be read from Table I. To estimate the degeneracy parameters for $[ErAl_3O_6]$ and $[Al_4O_6]$, x_{Er} and x_{Al}, I assume that only the ring states depicted in Fig. 1 are present and that there is one 6-member ring per Si site as in α quartz. This gives $x_{Er}=2$ [Fig. 1(a)] and $x_{Al}=14$ [Figs. 1(b) and 1(c)]. Although this choice of degeneracies is probably somewhat arbitrary considering the complexity of amorphous silica networks it seems reasonable to assume that the number of favorable configurations is higher for $[Al_4O_6]$ units than for $[ErAl_3O_6]$, since Al does not require as much interstitial space as the RE ions. Having fixed these parameters, it is now possible to calculate the critical Al/RE ratio r_c at which ΔF is zero. In Fig. 3 I have plotted this quantity as a function of Er concentration for various values of the temperature parameter. It can be seen that the r_c values for Er concentrations on the order of 10^{19} cm^{-3} are in the range between 4 and 12 for temperatures between 1200 and 1800 K. Experimentally, an Al/RE ratio of 10 is usually found to suppress Er clustering sufficiently well to allow for device fabrication. This is in reasonable accordance with the theoretical results, considering the approximative nature of the calculation.

Considering the energy of isolated Er ions compared to the clustered ones, a rough estimate can be obtained from the results of Ref. 2, where Er cluster formation was studied at temperatures around 1400 K. It was found that no clusters formed in regions where the Er_2O_3 concentration was below $\sim 10^{18}$ cm^{-3}. Assuming that the entropy term balances the difference in total energy at this concentration, one derives from Eq. (10) a total-energy difference of about 2.6 eV/Er_2O_3. Since the experiment in Ref. 2 was only able to distinguish clusters of a certain size this should be considered a lower limit on the energy difference. Thus, the energy of isolated Er atoms is much higher than either of the other states considered, and it seems fair to neglect their importance at the high concentrations of interest here.

When manufacturing RE-doped glass by processes such as the sol-gel or the PECVD method, subsequent heat treatment is a common recipe for increasing glass transparency by eliminating unwanted impurities. The usual strategy for increasing the attainable rare-earth concentration is to limit the duration and temperature of this heat treatment as much as possible in order to avoid diffusion and clustering of the RE ions. The thermodynamic reasoning applied above suggests that an alternative strategy may be to anneal at a very high temperature for a long time in order to attain thermodynamic equilibrium at a temperature high enough to favor dissolved RE ions. Systematic studies of clustering behavior under long anneals as a function of temperature and composition would constitute an appropriate verification experiment for this hypothesis.

C. Electronic structure

1. Charge distributions

The definition of charge transfer in partially ionic compounds is not a straightforward matter when using plane-wave expanded wave functions that do not lend themselves to the Mulliken population analysis commonly used with local orbitals. In a previous study of $Er_2Si_2O_7$ (Ref. 13) a procedure was suggested in which the charge inside some chosen sphere around a particular atom was compared to a reference charge constructed from overlapping free-atom densities, i.e.,

$$\Delta\rho = \int_{\text{sphere}} d\mathbf{r}[n(\mathbf{r}) - \rho_0(\mathbf{r})], \tag{17}$$

$$\rho_0(\mathbf{r}) = \sum_{\mathbf{R}} \sum_i \rho_{\text{at}}^i(\mathbf{r} - \mathbf{R} - \boldsymbol{\tau}_i), \tag{18}$$

ρ_{at}^i being the charge density of a free atom of type i. $\mathbf{R}$ are the Bravais lattice vectors, while the i sum runs over the atoms of the unit cell, and $\boldsymbol{\tau}_i$ are the position vectors of the atoms in the cell with $\mathbf{R}=\mathbf{0}$. $n(\mathbf{r})$ is the charge density in the solid state. In the present paper I will use sphere radii equal to the pseudization radii for the various atoms (1.8 a.u. for Al and 2.0 a.u. for Er), in which case n may be represented by the pseudodensity that preserves the moments (but not the radial shape) of the charge distribution inside the pseudization spheres.[13] It is important to note that the numbers obtained from this method depend entirely upon the choice of sphere radii, and values for different atom types cannot be compared in a meaningful way. On the other hand, differences between charge transfers to the same type of atom in different environments are revealed by the analysis.

The charge transfer results for Er are given in Table II. It can be seen that the numbers for Er in $Er_2Si_2O_7$ and in the $[ErAl_3O_6]$ impurity complex are similar, whereas the transfer of electrons away from Er is slightly smaller in crystalline Er_2O_3. To understand this difference one must consider the differences in the local environment of Er between the systems. In all three cases Er is bonded to three-coordinated O atoms, but the environment of these are dissimilar: In Er_2O_3 all O atoms are, of course, bonded to three Er ions, whereas

TABLE II. Charge transfer results (in units of e) for Er atoms in the compounds considered here. The charge of the electron is counted negative, i.e., a positive number means that electrons are transferred away from the atom in question.

System	Atom	$\Delta\rho$
$SiO_2:[ErAl_3O_6]$	Er(1)	0.293
$Er_2Si_2O_7$	Er(1)	0.290
Er_2O_3	Er(1)	0.284
	Er(2)	0.276

in $Er_2Si_2O_7$ each O neighbor of Er is bonded to two Er and one Si atom. Finally, in the $[ErAl_3O_6]$ complex most neighbors of Er are bonded to one Er, one Al, and one Si atom (one O atom exists which is bonded to two Si and Er). Now the amount of charge that Er is able to give off to a given O atom depend on the charge that this atom receives from its other neighbors. Since the valence *spd* levels of Er are higher in energy than the valence *sp* levels of Si, charge transfer from Er to O will be favored over charge transfer from Si to O. This means that the replacement of Er with Si in the next-nearest-neighbor shell of an Er atom will increase the charge transfer away from Er in accordance with the numerical results. The similarity between the $Er_2Si_2O_7$ and $[ErAl_3O_6]$ charge transfers then indicates that Er and Al have similar electronegativities, i.e., their valence levels are close in energy. If this is the case, one would expect that the charge transfer away from the substitutional Al nuclei is not strongly dependent on whether the interstitial ion is Al or Er. The results for Al charge transfers presented in Table III shows that this is indeed the case. This result unfortunately means that it will be difficult to distinguish the $[Al_4O_6]$ and $[ErAl_3O_6]$ states in Al spectroscopies that depend on the charge distribution (e.g., core level spectroscopy).

2. The eigenvalue spectrum

The Kohn-Sham eigenvalue spectrum of the $[ErAl_3O_6]$ impurity complex as calculated from Eq. (9) is shown in Fig. 4. The spectrum was obtained sampling only the Γ point in $\mathbf{k}$ space, since the small dispersion of the states due to the use of a finite supercell is not of interest here. A gaussian broadening of 0.2 eV has been used to smoothen the curves. The caveats from the charge transfer analysis apply here as well: The magnitude of projected state densities is a rather arbitrary quantity depending on the choice of sphere radii. Therefore the values for different elements are not directly com-

TABLE III. Charge transfer results for substitutional Al atoms in the $[ErAl_3O_6]$ and $[Al_4O_6]$ structures. The $[Al_4O_6]$ structure similar to $[ErAl_3O_6]$ [depicted in Fig. 1(c)] was used for the calculation. Signs and units are as in Table II.

Atom	$[ErAl_3O_6]$	$[Al_4O_6]$
Al1	0.154	0.162
Al2	0.160	0.160
Al3	0.159	0.150

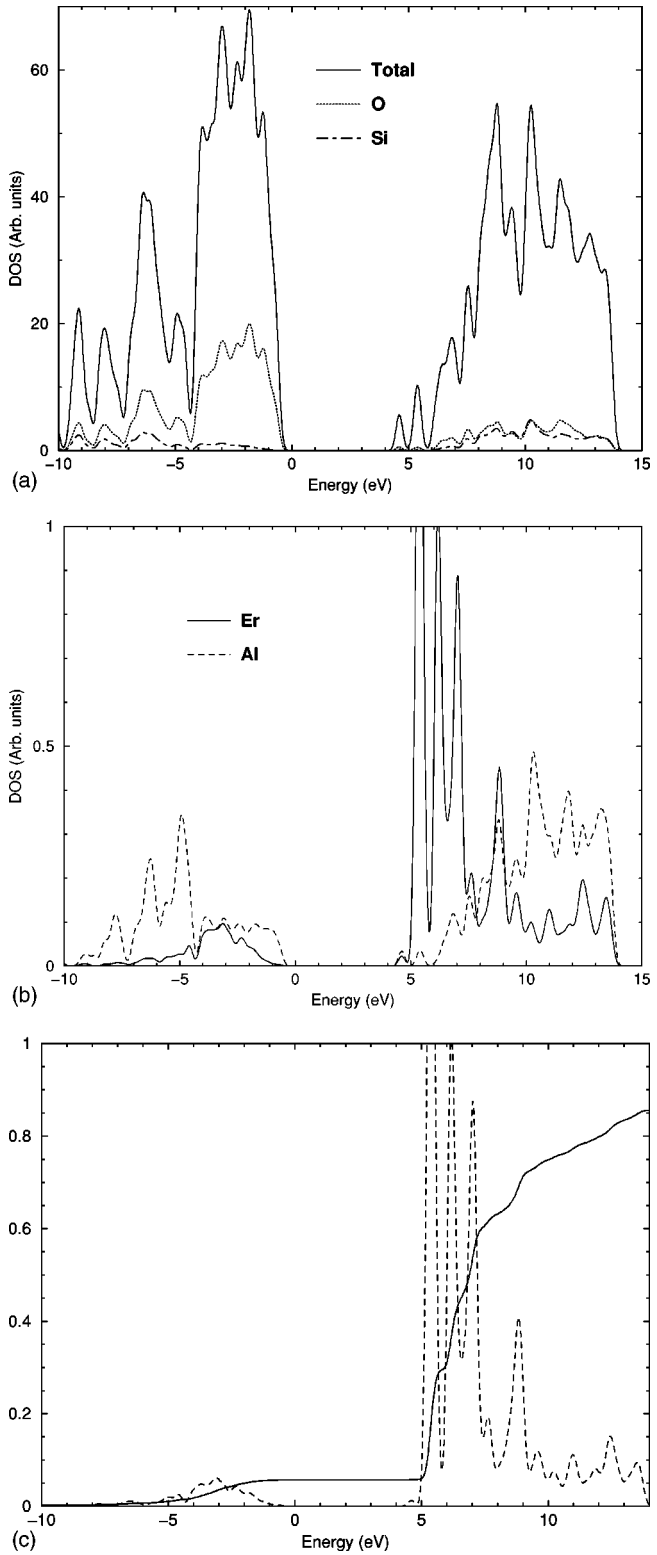

FIG. 4. Kohn-Sham eigenvalue spectra of the $[ErAl_3O_6]$ supercell. The total DOS along with the Si,O projections is shown in (a), while (b) gives the impurity-projected spectra. In (c) the projection upon the atomic Er 5d state is shown (dashed line), along with its cumulative integral (solid line).

parable, but for each element trends as a function of energy may yield information on the chemical bonding at work.

The total density of states (DOS) shown in Fig. 4(a) is dominated by Si and O related states, since these elements constitute the major part of the supercell. The valence bands are similar to those of pure silica: At low energies bonding Si-O states are found, whereas the top of the valence band is comprised of nonbonding O $2p$ states. In the conduction band, the antibonding states, distinguished from the bonding states by larger weight on Si and smaller weight on O, are found. Figure 4(b) shows the impurity-projected DOS. It can be seen that the Al projection is quite similar to that of Si, except for the fact that the bonding states are slightly higher in energy due to the higher position of the Al $3sp$ levels. On the other hand, the Er DOS shows additional features due to the presence of the $5d$ multiplet. The large Er peaks in the lower part of the conduction band are essentially $5d$ states, with some hybridization to the neighboring O atoms. In Fig. 4(c) the DOS projected onto the free-atom $5d$ eigenstate within the pseudization sphere (which closely resembles the DOS projected on the US-PP *d*-channel projector functions) is plotted together with its integrated weight. The latter has been divided by ten times the weight of the atomic orbital inside the sphere, so that if all the $5d$ weight was sampled the integral should reach unity. It can be seen from the figure that the $5d$ weight below the Fermi edge corresponds to less than one electronic state, whereas about six (including spin degeneracy) states appear in a narrow range between 5 and 7.5 eV in the conduction band. At higher energies states with a partial Er $5d$ character are found.

D. Electrostatic potentials and Judd-Ofelt theory

The influence of the electrostatic potential of a host material on rare-earth $4f$ multiplets (often referred to as ''ligand-field effects'') has been extensively discussed because of its importance in manufacturing active optical devices. The potential has two important effects: Firstly, it splits the free-ion J multiplets into a set of close-lying (typically within a few hundred cm^{-1}) energy levels, thus modifying the gain spectrum of an active material. And secondly, they provide a weak coupling of the $4f$ orbitals to the surrounding states, making transitions between different J multiplets dipole allowed. As it turns out, this effect controls the magnitudes of pump absorption and signal amplification. It is not the purpose of the present paper to provide a detailed account of atomic multiplet structure, or to sample the distribution of random environments available to a rare earth in glass, but rather to examine the validity of some assumptions commonly made when modeling ligand-field effects.

Ligand-field perturbations of free-ion multiplets are conveniently discussed using an angular-momentum expansion of the electrostatic potential around the nucleus in question, i.e.,

$$V_e(\mathbf{r}) = \sum_{lm} V_{lm}(r) Y_{lm}(\hat{\mathbf{r}}), \tag{19}$$

where Y_{lm} are the usual spherical harmonics. The even-l terms in the expansion (with $l=2,4,6$) contribute to the Stark

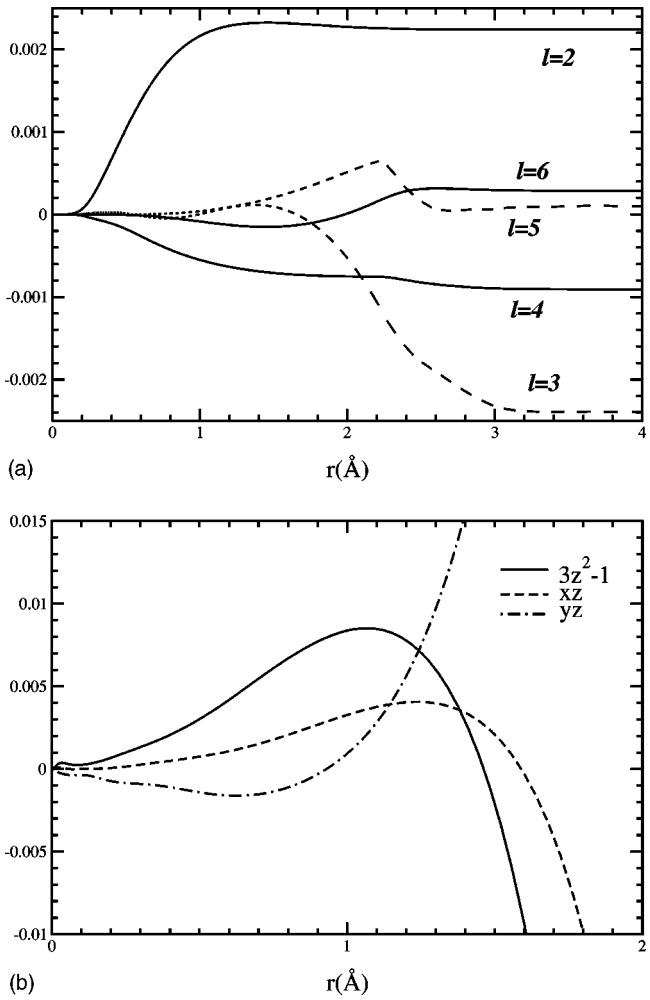

FIG. 5. Electrostatic potentials around the Er nucleus in the $[ErAl_3O_6]$ structure. In (a) the cumulative integrals of the $m=0$ radial potential functions weigthed with either the $4f$-$4f$ wavefunction product (for even l) or the $4f$-$5d$ product (odd l) are given. In (b), some of the $l=2$ radial potential components are shown. The potential is reported in atomic Hartree units.

splitting of the various $4f$ multiplets. When working to lowest order in perturbation theory, the splittings are solely determined by the matrix elements of the electrostatic potential between different states in a given $4f$ J multiplet. The effect of the odd-l terms in the potential is different but no less important: They couple the $4f$ states to the components of surrounding states with opposite parity, so that finite dipole matrix elements will exist between the resulting eigenstates. This is not the case for a ''pure'' $4f$ multiplet because all $4f$ states have the same parity. The surrounding states to which the $4f$ orbitals couple can either be other atomiclike rare-earth orbitals (e.g., the $5d$ multiplet), host states, or a mixture of both.

In Fig. 5(a) the functions

$$f_l(r) = \int_0^r dr' r'^2 V_{l0}(r') R_1(r') R_2(r') \tag{20}$$

are plotted for $l=2$–6. For even l (solid lines), the radial wave functions, R, are both taken to be the free-atom Er $4f$

Kohn-Sham wave function as calculated with the GGA functional, whereas for the odd l values (dotted lines), the product of Er $4f$ and $5d$ wave functions is used. Such a plot reveals the spatial region which is of interest when calculating matrix elements of the electrostatic potential. It can be seen that the even-l f-f matrix elements (relevant for calculating Stark splittings) have support at shorter radii than the odd-l f-d matrix elements because the f-f wave function product has shorter range than the f-d product. In addition, the main contribution to the integral is shifted outwards with increasing l, since the highly asymmetric potential components have small weight in the Er core region.

When modeling the Stark splitting of rare earths in glasses it is often assumed that the $4f$ states are corelike in the sense that the nonspherical part of the electrostatic potential can be modeled by the potential from a set of point charges representing the ligand ions.[17,18] Thus, the overlap of the $4f$ states with the valence electron density of both the surrounding ions and the rare earth $5d$ and $6sp$ orbitals is neglected. From Fig. 5(a) this is clearly an inadequate approximation for the $l=6$ (and to a lesser extent $l=4$) components of the potential where a significant contribution to the matrix element comes from the region around the first neighbor shell of Er ($r=2.35$ Å). On the other hand, the matrix element of the $l=2$ component is essentially determined within a radius of 1 Å. However, even at this range the radial potential functions do not resemble that of a set of point charges, which would simply be proportional to r^2. In Fig. 5(b) some of the $l=2$ potentials are plotted in the cube harmonic representation, in which the radial functions are all real. Close to the Er nucleus the potentials show structure arising from the shape of the Er valence orbitals, indicating that the potential in this range is significantly affected by the local charge density. Between 0.2 and 1 Å where the major contribution to the f-f matrix element is found the potential does show a monotonous behavior, but only superficially resembles an r^2 function. Thus, even for the most localized contribution to the Stark perturbation matrix, the approximation of a point charge electrostatic potential does not seem well justified.

The coupling of the $4f$ states to the surrounding orbitals is usually discussed within the framework of Judd-Ofelt theory,[19,20] which conveniently condenses the ligand-field effects on the $4f$ multiplet into three parameters that can either be calculated directly from a model of the ligand field or, as is most often done, fitted to spectroscopic data for various materials. The Judd-Ofelt theory assumes that the $4f$ states only couple to atomiclike rare-earth orbitals (most notably $5d$) and that the rare-earth ion is fully ionized so that no electron transfer *from* the valence orbitals *to* the $4f$ manifold needs consideration. Extensive use of angular momentum sum rules along with certain degeneracy assumptions then produce the desired simplifications. In a solid host material one should, of course, in principle consider coupling to hybridized states involving electron transfer both to and from the $4f$ multiplet, so it is important to clarify the extent to which the approximations made in Judd-Ofelt theory are reasonable.

From the orbital-projected DOS in Fig. 4(c) it can be seen that several states with high Er $5d$ character are found near the bottom of the conduction band in the $[ErAl_3O_6]$ structure. On the other hand, a substantial part of the $5d$ weight is present at higher energies in more hybridized states. Therefore, the use of atomic sum rules for the eigenstates in the solid is only partially justified: It may serve as a reasonable first approximation, but cannot be expected to yield quantitative accuracy. Concerning the possibility of coupling to other states than the Er valence orbitals it is interesting to notice that the main contribution to the odd-l $4f$-$5d$ matrix elements in Fig. 5(a) comes from the region of the first Er coordination shell, where the strong asymmetry of the potential more than makes up for the decay of the $4f$ orbital. Therefore one can expect that the coupling to other states, localized mainly on the neighboring atoms, will have a similar magnitude. These couplings could not only produce electron transfer from the $4f$ multiplet into the antibonding Si,Al-O states, but also electron transfer from the occupied O $2p$ nonbonding (or Si,Al-O bonding) states to the $4f$ multiplet. Since these are extended band states their contribution to the $4f$ hybridization function will be much broader in energy than that of the localized Er $5d$ states, but their cumulative weight within an energy window of 5–10 eV may nevertheless be comparable to that of the $5d$ contribution.

Apart from the shape and magnitude of the nonspherical electrostatic potential an important parameter for $4f$ hybridization is the energy required for transferring an electron from the $4f$ manifold to the surroundings or vice versa. I have calculated the f^{11}-f^{12} and f^{11}-f^{10} excitation energies along the lines described in Sec. II. In the case of f^{11}-f^{10} excitation the electron added to the conduction band is almost completely localized in a state of Er $5d$ character. The excitation energy required is found to be 11.04 eV. When f^{11}-f^{12} excitation is considered the hole injected into the valence band primarily goes into nonbonding O $2p$ states. The hole is only partially localized around the Er impurity: About half of the total spin density found within the pseudization spheres of the 48 O atoms in the supercell is located on the 8 O atoms nearest to Er. As has been discussed previously in the case of a substitutional Al impurity,[21,22] this delocalization is an artifact of the GGA approximation: The spurious self-interaction of the hole arising from the approximate energy functional prevents the hole from localizing on a particular O atom. A more realistic picture of the available hole states is that they are localized on individual O atoms, but this does not disturb the conclusion that a considerable number of states will be available within a limited energy range. The energy required for the f^{11}-f^{12} excitation is as small as 0.87 eV in the calculation. In spite of the approximative nature of the GGA method, the order-of-magnitude difference between f^{10} and f^{12} excitation energies is remarkable. Since the bandwidth of the nonbonding O $2p$ states is only ~ 5 eV, it must be concluded that f^{11}-f^{12} excitations can be expected to play a considerable role in determining the dipole matrix elements between different J states in a rare-earth $4f$ multiplet.

IV. CONCLUSIONS

In conclusion, I have presented a microscopic model of an Er-Al complex in silica which could be responsible for dis-

solution of Er clusters upon Al codoping. I have demonstrated through parameter-free DFT calculations that the model predicts local environments for Er and Al in good agreement with EXAFS results, and that the total energy of the complex is slightly higher than that of a phase-separated state having the structure of crystalline $Er_2Si_2O_7$. This could explain why the Al/Er ratio usually has to be around 10 to ensure complete cluster dissolution although only 3 Al ions are required to dissolve one Er ion.

An analysis of the Kohn-Sham eigenvalue spectra and the electrostatic potential around Er in the Er-Al impurity complex lends only limited support for the approximations underlying the Judd-Ofelt theory of Er spectra in solutions. Furthermore, the commonly used assumption that the shape of the electrostatic potential can be modeled by the potential from a set of surrounding point charges is not supported by the present calculations.

ACKNOWLEDGMENTS

Fruitful discussions with S. Guldberg-Kjær, I. Byriel, M. Kristensen, and K. Stokbro are gratefully acknowledged.

[1] S. Sen and J. Stebbins, J. Non-Cryst. Solids **188**, 54 (1995).
[2] M.W. Sckerl, S. Guldberg-Kjær, M.R. Poulsen, P. Shi, and J. Chevallier, Phys. Rev. B **59**, 13 494 (1999).
[3] E. Delevaque, T. Georges, M. Monerie, P. Lomouler, and J.F. Bayon, IEEE Photonics Technol. Lett. **5**, 73 (1993).
[4] K. Arai, H. Namikawa, K. Kumata, T. Honda, Y. Ishii, and T. Handa, J. Appl. Phys. **59**, 3430 (1986).
[5] K. Arai, S. Yamasaki, J. Isoya, and H. Namikawa, J. Non-Cryst. Solids **196**, 216 (1996).
[6] S. Sen, J. Non-Cryst. Solids **261**, 226 (2000).
[7] J. Lægsgaard, Phys. Rev. B **65**, 174104 (2002).
[8] J.P. Perdew, J.A. Chevary, S.H. Vosko, K.A. Jackson, M.R. Pederson, D.J. Singh, and C. Fiolhais, Phys. Rev. B **46**, 6671 (1992).
[9] P. Hohenberg and W. Kohn, Phys. Rev. **136**, B864 (1964).
[10] W. Kohn and L. Sham, Phys. Rev. **140**, A1133 (1965).
[11] D. Vanderbilt, Phys. Rev. B **41**, 7892 (1990).
[12] K. Laasonen, A. Pasquarello, R. Car, C. Lee, and D. Vanderbilt, Phys. Rev. B **47**, 10 142 (1993).
[13] J. Lægsgaard and K. Stokbro, Phys. Rev. B **63**, 075108 (2001).
[14] P.E. Blöchl, Phys. Rev. B **50**, 17 953 (1994).
[15] G. Kresse and D. Joubert, Phys. Rev. B **59**, 1758 (1999).
[16] F. d'Acapito, S. Mobilio, L. Santos, and R.M. Almeida, Appl. Phys. Lett. **78**, 2676 (2001).
[17] G. Cormier, J.A. Capobianco, C.A. Morrison, and A. Monteil, Phys. Rev. B **48**, 16 290 (1993).
[18] K. Soga, H. Inoue, and A. Makishima, J. Non-Cryst. Solids **274**, 69 (2000).
[19] B.R. Judd, Phys. Rev. **127**, 750 (1962).
[20] G.S. Ofelt, J. Chem. Phys. **37**, 511 (1962).
[21] G. Pacchioni, F. Frigoli, D. Ricci, and J.A. Weil, Phys. Rev. B **63**, 054102 (2001).
[22] J. Lægsgaard and K. Stokbro, Phys. Rev. Lett. **86**, 2834 (2001).